

Hug and Hop: a discrete-time, non-reversible Markov chain Monte Carlo algorithm

Matthew Ludkin^{*1} and Chris Sherlock¹

¹Lancaster University

May 10, 2022

Abstract

We introduced the Hug and Hop Markov chain Monte Carlo algorithm for estimating expectations with respect to an intractable distribution π . The algorithm alternates between two kernels: *Hug* and *Hop*. *Hug* is a non-reversible kernel that uses repeated applications of the bounce mechanism from the recently proposed Bouncy Particle Sampler to produce a proposal point far from the current position, yet on almost the same contour of the target density, leading to a high acceptance probability. *Hug* is complemented by *Hop*, which deliberately proposes jumps between contours and has an efficiency that degrades very slowly with increasing dimension. There are many parallels between *Hug* and Hamiltonian Monte Carlo (HMC) using a leapfrog integrator, including an $\mathcal{O}(\delta^2)$ error in the integration scheme, however *Hug* is also able to make use of local Hessian information without requiring implicit numerical integration steps, improving efficiency when the gains in mixing outweigh the additional computational costs. We test *Hug* and *Hop* empirically on a variety of toy targets and real statistical models and find that it can, and often does, outperform HMC on the exploration of components of the target.

1 Introduction

Markov chain Monte Carlo (MCMC) algorithms approximate expectations under an un-normalised target distribution of π by simulating a Markov chain with π as its stationary distribution then computing empirical averages over the simulated values of the chain. Historically MCMC has been based on reversible Markov kernels such as the Metropolis-Hastings kernel (Hastings, 1970) and special cases and variations of this (e.g. Brooks et al., 2011) since it is straightforward to ensure that these target π . However, there has been much recent interest in non-reversible kernels (e.g. Bouchard-Côté et al., 2018; Fearnhead et al., 2018) which have the potential both in practice and in theory to be more efficient than their reversible counterparts (Neal, 1998; Diaconis et al., 2000; Bierkens, 2015; Ma et al., 2018). A particular continuous-time non-reversible algorithm, the Bouncy Particle Sampler (BPS) (Peters and de With, 2012; Bouchard-Côté et al., 2018) and variations such as the coordinate sampler Wu and Robert (2018) and the Discrete Bouncy Particle Sampler (DBPS Sherlock and Thiery (2017); Bouchard-Côté et al. (2018)) and variations on both the BPS and DBPS (Vanetti et al., 2017), uses occasional reflections of a velocity in the hyperplane perpendicular to the current gradient to eliminate (for continuous-time versions) or substantially reduce (discrete-time versions) rejections of proposed moves.

The BPS and its variants appear to be very efficient when examining individual components of the target, however certain functionals of the Markov chain, X , and in particular $\log \pi(X)$, mix much more slowly than the individual components, whether the algorithm acts in continuous-time (Bierkens et al., 2018) or discrete-time (Sherlock and Thiery, 2017). We turn this fundamental problem with bouncy particle samplers to our advantage.

^{*}Corresponding author. This work was supported by EPSRC grant number EP/P033075/1

We introduce a novel, discrete-time, non-reversible sampling algorithm which itself consists of two accept-reject MCMC kernels, applied in alternation. Given a current value, the first kernel uses the bounce mechanism of the BPS/DPBS to evolve a skew-reversible approximation to an exact dynamical system (1) that moves at constant speed along a level set of π so as to produce a proposal point that is far from the current position, yet on almost the same posterior contour, leading to a high acceptance probability; we denote this contour-hugging kernel *Hug*. We emphasise that Hug does not use a geodesic integrator such as SHAKE or RATTLE (e.g. Leimkuhler et al., 2004); these integrators approximate the dynamics whilst preserving a constraint exactly, and use implicit schemes, whereas hug is fully explicit and approximates both the dynamics and the constraint.

The second kernel complements the first by focusing on moving between contours. It encourages the next state of the Markov chain to lie on a different contour by proposing a new point from a distribution with high variance in the gradient direction, and lower variance in directions perpendicular to the gradient; we denote this kernel *Hop*, and the combination of the two *Hug and Hop*.

Hug is introduced formally in Section 2.1, where we also prove (Theorem 1) that it enjoys the same $\mathcal{O}(\delta^2)$ integration error as Hamiltonian Monte Carlo (HMC, e.g. Neal, 2011) implemented using the standard leapfrog integrator. There are a number of close analogies between Hug and HMC which we explore in more detail in Section 2.3, where we also point out that, unlike HMC, while evolving the dynamics, the standard version of Hug can be enhanced via an *explicit* scheme to use the local Hessian and account for local curvature or shape. Hop, described in Section 2.2, is a variation on the Directional Metropolis-Hastings algorithm of Mallik and Jones (2017), adjusted specifically cater to movements almost parallel with the gradient vector. As proved in Theorem 2 and demonstrated empirically in the simulation study that follows, this brings substantial benefits in terms of robustness to increasing dimension. In simulation studies on toy targets in Section 3 and real statistical examples in Section 4, we find that Hug and Hop is often more efficient than HMC in terms of the effective sample size (ESS) of individual components of the target, but less efficient in terms of the ESS of the functional $\log \pi(X)$. This is, perhaps, unsurprising since HMC aims to preserve the total energy, rather than $\log \pi$, and alters the magnitude of the velocity as the potential, $-\log \pi$, changes; moreover it has a continual impetus to move down the gradient, thus changing $\log \pi$.

1.1 Notation

Throughout the article the target is assumed to have a density of π with respect to Lebesgue measure. The log-density is denoted by $\ell(x) = \log \pi(x)$ and its gradient and Hessian are denoted by $g(x) = \nabla \ell(x)$ and $H(x) = [\partial^2 \ell / \partial x_i \partial x_j]$, while the unit gradient vector is denoted by $\hat{g}(x) = g(x) / \|g(x)\|$. For some small $\epsilon > 0$, when the negative Hessian is positive definite with all eigenvalues above ϵ , we write $\Sigma(x) = -H(x)^{-1}$. Otherwise, we set $\Sigma(x) = -L^\top (|1/\Lambda| + \epsilon I_d) L$, where $L^\top \Lambda L$ is the spectral decomposition of H and $|1/\Lambda|$ denotes the (diagonal) matrix whose elements are the reciprocal of the absolute values of the corresponding elements of Λ . $\Sigma(x)$ can therefore be considered as a local variance-covariance matrix with eigenvalues informed by the local curvature along each principal component, whether this is positive or negative. Given $\Sigma(x)$, the matrix $A(x)$ always denotes a $d \times d$ matrix square-root of $\Sigma(x)$; i.e., $A(x)^\top A(x) = \Sigma(x)$.

2 The Hug and Hop kernels

2.1 Hug

Consider a particle initialised at x_0 with a velocity of $v_0 \perp g(x_0)$ and evolving for a time T according to

$$\begin{aligned} \frac{dx}{dt} &= v, \\ \frac{dv}{dt} &= -\frac{v^\top H(x)v}{\|g(x)\|^2} g(x). \end{aligned} \tag{1}$$

Since

$$\frac{d}{dt}(v^\top g) = v^\top \frac{dg}{dt} + \frac{dv^\top}{dt} g = v^\top \frac{dg}{dx} v - \frac{v^\top H v}{\|g\|^2} g^\top g = 0,$$

v remains perpendicular to g , and hence to dv/dt , so $d\|v\|/dt = 0$. The particle’s speed is constant but its velocity is continually adjusted so that it is always perpendicular to the gradient of $\log \pi$, and hence the particle never leaves the particular surface of $\log \pi$ from which it started. The Hug kernel is a time-discretisation of the (generally intractable) dynamics in (1); it repeatedly uses the reflection move of the Bouncy Particle Sampler,

$$R(v; g) = v - 2(v^\top \widehat{g})\widehat{g}, \quad (2)$$

to ‘bounce’ the current velocity off the hyperplane tangent to the local gradient. The proposal mechanism from a current sample point x_0 samples an initial velocity, v_0 , from a proposal distribution q which satisfies $q(v | x) = q(-v | x)$ but need not and should be forced to produce initial velocities perpendicular to the current gradient. The dynamics in (1) are then approximated for a time T and a discretisation interval of $\delta = T/B$ by repeating the following B times: firstly move to $x'_b := x_b + \delta v_b/2$, then reflect the velocity in the gradient at x'_b : $v_{b+1} = R(v_b; g(x'_b))$, and finally move to $x_{b+1} = x'_b + \delta v_{b+1}/2$. Algorithm 1 describes a single application of the kernel, P_{hug} .

Algorithm 1 Contour-hugging.

Require: integration time, T ; number of steps, B ; initial value, x_0 ; symmetric proposal density $q(\cdot|x)$.

$\delta \leftarrow \lfloor T/B \rfloor$.

Draw velocity $v_0 \sim q(\cdot|x_0)$.

for $b = 0, \dots, B - 1$ **do**

Move to $x'_b = x_b + \delta v_b/2$.

Reflect: $v_{b+1} \leftarrow R(v_b; g(x'_b))$.

Move to $x_{b+1} = x'_b + \delta v_{b+1}/2$.

end for

Compute $\log \alpha = [\ell(x_B) + \log q(v_B|x_B)] - [\ell(x_0) + \log q(v_0|x_0)]$.

Accept x_B as the new position with probability α ; otherwise remain at x_0 .

P_{hug} , can be viewed as the composition of two reversible kernels each of which preserves detailed balance with respect to the extended target of $\tilde{\pi}(x, v) := \pi(x)q(v | x)$. Let P_{hugR} be exactly as P_{hug} , except that the proposed velocity is $-v_B$ rather than v_B , and let $P_{\text{flip}} : (x, v) \rightarrow (x, -v)$, so that $P_{\text{hug}} = P_{\text{flip}}P_{\text{hugR}}$. Since q is symmetric, P_{flip} preserves $\tilde{\pi}$. To see that P_{hugR} preserves $\tilde{\pi}$, and hence so does P_{hug} , we first consider the inner loop of P_{hugR} . The transformation involves a reflection of velocity, sandwiched between two translations of position; each of these individual transformations has a Jacobian of 1 and so the Jacobian for the entire transformation from (x_0, v_0) to $(x_B, -v_B)$ is also 1. Hence, if X is stationary, the joint density of $(x_B, -v_B)$ is equal to $\pi(x_0)q(v_0 | x_0)$. Secondly, the inner loop is skew symmetric, so that starting from $(x_B, -v_B)$ and repeating the inner loop B times, then flipping the velocity would lead back to (x_0, v_0) , so, at stationarity, the joint density for the reverse move is $\pi(x_B)q(-v_B | x_B) = \pi(x_B)q(v_B | x_B)$. Hence the acceptance probability α in Algorithm 1 leads to P_{hugR} being reversible with respect to $\pi(x)q(v | x)$.

To show why the hug kernel is effective as an MCMC proposal mechanism, consider the step from x_b to x_{b+1} . Taylor expanding about the bounce point x'_b , and noting that $x'_b - x_b = \frac{\delta}{2}v_b$ and $x_{b+1} - x'_b = \frac{\delta}{2}v_{b+1}$ gives:

$$\begin{aligned} \ell(x_b) &= \ell(x'_b) - \frac{\delta}{2}v_b^\top g(x'_b) + \frac{\delta^2}{8}v_b^\top H(x_b^+)v_b, \\ \ell(x_{b+1}) &= \ell(x'_b) + \frac{\delta}{2}v_{b+1}^\top g(x'_b) + \frac{\delta^2}{8}v_{b+1}^\top H(x_{b+1}^-)v_{b+1}, \end{aligned}$$

where x_b^+ lies on the line between x_b and x'_b , and x_{b+1}^- lies on the line between x'_b and x_{b+1} . Now $(v_b + v_{b+1})^\top g(x'_b) = 2v_b^\top g(x'_b) - 2(v_b^\top \widehat{g}(x'_b))\|g(x'_b)\| = 0$, so:

$$\ell(x_{b+1}) - \ell(x_b) = \frac{\delta^2}{8} [v_{b+1}^\top H(x_{b+1}^-)v_{b+1} - v_b^\top H(x_b^+)v_b]. \quad (3)$$

Integrating for a time $T = B\delta$ requires T/δ such steps and might be supposed to lead to an error of $\mathcal{O}(\delta)$. However, if the behaviour of the Hessian is controlled, then the successive error terms comprise an

almost-telescoping sum and the full integration also has an error of $\mathcal{O}(\delta^2)$. We choose to require conditions based on the induced ℓ_2 -norm of the Hessian and changes in the Hessian. For a matrix M , $\|M\|_I = \sup_{x \in \mathbb{R}^d / \{0\}} \|Mx\|_2 / \|x\|_2$.

Condition 1 (Lipshitz-continuous Hessian).

There exists some $\gamma > 0$, such that $\|H(y) - H(x)\|_I \leq \gamma \|y - x\|$ for all $x, y \in \mathbb{R}^d$.

Condition 2 (Bounded Hessian).

There exists some $\beta > 0$, such that $\sup_{x \in \mathbb{R}^d} \|H(x)\|_I \leq \beta < \infty$.

These two conditions lead to the following result, which is proved in Appendix A.1.

Theorem 1. Consider a target π such that the Hessian $H(x)$ of $\ell(x) = \log \pi(x)$ satisfies Condition 1 and Condition 2. For a single iteration of Hug (Algorithm 1) with initial velocity v_0 ,

$$|\ell(x_B) - \ell(x_0)| \leq \frac{1}{8} \delta^2 \|v_0\|^2 (2\beta + \gamma D),$$

where $D = \|v_0 T\|$ is the total distance travelled in time T .

The only velocity changes are reflections, so $\|v_B\| = \|v_0\|$. Thus if q is isotropic and independent of x , rather than simply symmetric, then $\alpha = 1 \wedge \exp[\ell(x_B) - \ell(x_0)] = \mathcal{O}(\delta^2)$. In practice, for the standard version of P_{hug} we do not choose to let q depend on x , and potential global anisotropy can be dealt with by pre-conditioning, as we now discuss.

Typically, preconditioning according to the overall shape of the target can lead to large improvements in efficiency (e.g. Roberts and Rosenthal, 2001; Sherlock et al., 2010). As in many other algorithms, such as the RWM (Hastings, 1970) or MALA (Besag, 1994; Roberts and Rosenthal, 1998), the shape of the proposal distribution should aim to mimic the shape of the target and it might be preferable to employ an elliptically symmetric proposal such as $V_b | x_b \sim \mathsf{N}(x_b, \Sigma)$, where Σ is some approximation to the variance matrix of X under π . The transformed target $\tilde{x} = (A^{-1})^\top x$, where $A^\top A = \Sigma$, should be more isotropic than the original target and a natural, isotropic proposal on this target is equivalent to the elliptical proposal on the original target given above. However, the bounce kernel also has a reflection move, and the standard bounce dynamics, which have no *a priori* understanding of the target shape should be applied in the transformed, approximately isotropic, space. Since $\tilde{g}(\tilde{x}) = Ag(x)$, this is equivalent to applying the following reflection operator in the original space:

$$\mathsf{R}_{\text{prec}}(v; g) = v - 2 \frac{(v^\top g)}{g^\top \Sigma g} \Sigma g. \quad (4)$$

The overall effect of preconditioning can be understood in terms of Theorem 1 and Conditions 1 and 2 as effectively reducing γ and β for a fixed $\|v_0\|$ and T , thus allowing a larger step size, δ .

As mentioned in Section 1, the Hug proposal can make explicit use of the Hessian during the velocity bounces, leading to a position-dependent preconditioning using $A(x)$ as defined in Section 1.1. For each bounce point, x' , rather than bouncing off the plane tangential to the gradient at x' , the kernel P_{hugH} first transforms space, leading to $\tilde{v}_b = (A(x')^\top)^{-1} v_b$; the reflection (2) is then carried out in the transformed space and then the velocity in the original space is obtained as $v_{b+1} = A(x')^\top \tilde{v}_{b+1}$. This is equivalent to applying (4) in the original space, with $\Sigma = \Sigma(x')$ as defined in section 1.1. This kernel, P_{hugH} , is also skew-reversible and has a Jacobian of 1. The only difference when compared to Algorithm 1 is the reflection operation. This also has a Jacobian of 1 (it is a reflection) and only uses information available at x' . Therefore, P_{hugH} is skew-reversible and volume-preserving. Unlike for P_{hug} where we usually choose $q(v | x)$ to be independent of position, for P_{hugH} , typically $q(v | x)$ depends on x through the Hessian at x .

Interestingly, a position-dependent transformation improves on the $\mathcal{O}(\delta^2)$ error for a single step in (3); however there is no ‘almost-telescoping’ to improve the overall order of the algorithm. As with simple preconditioning, efficiency gains arise from the effective reduction of β and γ . Proposition 1 is proved in Appendix A.2.

Proposition 1. If $H(x)$ satisfies Condition 1, $|\ell(x_{b+1}) - \ell(x_b)| \leq \frac{\gamma \delta^3}{8} \left\{ \|v_{b+1}\|^3 + \|v_b\|^3 \right\}$.

Contour-hugging alone will not explore the target well since, by design, all points lie approximately on the same contour of the target. To ensure satisfactory exploration of the target, the contour-hugging kernel is complemented by a contour-hopping kernel which aims to propose points on different contours; this is the subject of Section 2.2.

2.2 Hop

We now describe the *hop* kernel, which makes reversible moves between contours by using gradient information to deliberately direct most of the movement of a random-walk-style proposal either up or down in the gradient direction. For a given scaling, λ_x , of the along-gradient component of the kernel, typically, the steeper the gradient itself at x , the larger the resulting change in log-posterior between the proposed value, y and the current value, x . Motivated by the wish to control the magnitude of $\ell(y) - \ell(x)$, when $\|g(x)\|$ is large we decrease the overall scaling in proportion to $\|g(x)\|$.

The Hop algorithm uses the proposal distribution:

$$Y \mid X = x \sim \text{MVN} \left(x, \frac{1}{\|g(x)\|^2} B(x) \right) \quad \text{with} \quad B(x) = \mu^2 I + (\lambda^2 - \mu^2) \hat{g}(x) \hat{g}(x)^\top. \quad (5)$$

Now, $\hat{g}(x)^\top B(x) \hat{g}(x) = \lambda^2$ and for any unit vector $e \perp \hat{g}(x)$, $e^\top B(x) e = \mu^2$, so with respect to any orthonormal basis that starts with $\hat{g}(x)$, $\text{Var}(Y \mid x) = \text{diag}(\lambda^2, \mu^2, \dots, \mu^2) / \|g(x)\|^2$. The portion of the proposal perpendicular to $\hat{g}(x)$ is an isotropic Gaussian with a scaling of μ and along the gradient line the proposal is Gaussian with a scaling of λ .

Given the interpretation immediately following (5), both $B(x)^{-1}$ and $B(x)^{1/2}$ have tractable forms, enabling fast and easy simulation and calculations of the contribution to r_{hop} :

$$B(x)^{-1} = \frac{1}{\mu^2} I + \left(\frac{1}{\lambda^2} - \frac{1}{\mu^2} \right) \hat{g}(x) \hat{g}(x)^\top, \quad (6)$$

$$B(x)^{1/2} = \mu I + (\lambda - \mu) \hat{g}(x) \hat{g}(x)^\top. \quad (7)$$

If $\mu = 0$ then a proposed point y will have an acceptance probability of zero, unless the gradient $g(y)$ is parallel to $g(x)$. This will generally not be the case, thus a strictly positive value for μ will be required.

The Metropolis-Hastings acceptance probability is $\alpha_{hop}(x, y) = 1 \wedge r_{hop}(x, y)$, where the acceptance ratio, r_{hop} satisfies:

$$\begin{aligned} \log r_{hop}(x, y) &= \ell(y) - \ell(x) + \log \text{MVN} \left(x; y, B(y) / \|g(y)\|^2 \right) - \log \text{MVN} \left(y; x, B(x) / \|g(x)\|^2 \right) \\ &= \ell(y) - \ell(x) + \frac{d}{2} \log \frac{\|g(y)\|^2}{\|g(x)\|^2} - \frac{1}{2} (y - x)^\top \left[\|g(y)\|^2 B_y^{-1} - \|g(x)\|^2 B_x^{-1} \right] (y - x), \\ &= \ell(y) - \ell(x) + \frac{d}{2} \log \frac{\|g(y)\|^2}{\|g(x)\|^2} - \frac{1}{2\mu^2} \|y - x\|^2 \left[\|g(y)\|^2 - \|g(x)\|^2 \right] \\ &\quad - \frac{1}{2} \left(\frac{1}{\lambda^2} - \frac{1}{\mu^2} \right) \left\{ [(y - x)^\top g(y)]^2 - [(y - x)^\top g(x)]^2 \right\}. \end{aligned} \quad (8)$$

using (6), and since $\det(B(x)) = \lambda\mu^{d-1}$ is independent of x .

If the scaling by $\|g(x)\|^2$ were omitted, the Hop algorithm would be a special case of the Directional Metropolis-Hastings algorithm of Mallik and Jones (2017), which also allows for a MALA-like offset of the proposal mean. However, unlike the algorithm in Mallik and Jones (2017), the Hop algorithm is specifically intended for jumping between contours. As we shall see in Theorem 2 below, which is proved in Appendix C, and the simulations in Section 3, the position-dependent scaling brings enormous (and, perhaps, unexpected) gains in efficiency for typical targets.

Theorem 2. Let $\{\gamma_i^{(d)}\}_{i=1, d=2}^{d, \infty}$ be a triangular sequence of independent and identically distributed random variables with positive support and $\mathbb{E}[\gamma^3] < \infty$; let $\{\Gamma^{(d)}\}_{d=2}^\infty$ be the sequence of $d \times d$ matrices with $\Gamma^{(d)} =$

$\text{diag}(\gamma_1^{(d)}, \dots, \gamma_d^{(d)})$. Consider a sequence of Gaussian targets, $\{\pi^{(d)}\}_{d=2}^\infty$, defined as

$$\pi^{(d)}(x^{(d)}) = (2\pi)^{-d/2} \det(\Gamma^{(d)})^{1/2} \exp\left[-\frac{1}{2}x^{(d)\top}\Gamma^{(d)}x^{(d)}\right],$$

and let $\alpha_{hop}^{(d)}(x^{(d)}, y^{(d)})$ be the corresponding acceptance probability as defined in (8). Then as $d \rightarrow \infty$

$$\lim_{d \rightarrow \infty} \mathbb{E}\left[\alpha_{hop}^{(d)}(\bar{X}^{(d)}, \bar{Y}^{(d)})\right] = 2\Phi\left(-\frac{\mu^2}{2\lambda}\right). \quad (9)$$

Furthermore, with $\mu^2 = \kappa\lambda$ for any fixed κ , and with $\lambda = o(\sqrt{d})$ yet $\lambda \geq b$ for some $b > 0$,

$$\mathbb{E}\left[\alpha_{hop}^{(d)}(X^{(d)}, Y^{(d)})\right] = 2\Phi\left(-\frac{\kappa}{2}\right) + \mathcal{O}\left(\frac{\lambda}{\sqrt{d}}\right).$$

As for the hug algorithm in Section 2.1, the Hop algorithm can be improved by transforming space using local curvature information, then performing the Hop proposal in the new space. Using the notation from Section 1.1 a point x is mapped to $\tilde{x} = (A(x)^{-1})^\top x$ and the gradient, $\tilde{g}(x)$ is mapped to $A(x)g(x)$. Thus, $\|\tilde{g}(x)\|^2 = g(x)^\top \Sigma(x)g(x)$ and the Hessian version of the Hop algorithm proposes points:

$$Y|X = x \sim \text{MVN}\left(x, \frac{1}{g(x)^\top \Sigma(x)g(x)} \left(\mu^2 \Sigma(x) + (\lambda^2 - \mu^2) \frac{\Sigma(x)g(x)g(x)^\top \Sigma(x)^\top}{g(x)^\top \Sigma(x)g(x)}\right)\right) \quad (10)$$

For a proposed point y from x , the log-acceptance ratio for a Hop using Hessian information is:

$$\begin{aligned} \log r_{hopH} &= \ell(y) - \ell(x) + \frac{d}{2} \log \frac{\|\tilde{g}(y)\|^2}{\|\tilde{g}(x)\|^2} + \frac{1}{2} \log \frac{\det(\Sigma(x))}{\det(\Sigma(y))} \\ &\quad - \frac{1}{2\mu^2} (y-x)^\top \left(\|\tilde{g}(x)\|^2 H_x - \|\tilde{g}(y)\|^2 H_y\right) (y-x) \\ &\quad - \frac{1}{2} \left(\frac{1}{\lambda^2} - \frac{1}{\mu^2}\right) \left([\!(y-x)^\top g(y)\!]^2 - [\!(y-x)^\top g(x)\!]^2\right) \end{aligned} \quad (11)$$

We now explore the robustness of the conclusions from Theorem 2 to deviations from the multivariate Gaussian target by considering a set of targets with position-dependent Hessians. In practise, to avoid numerical issues with small $\|g\|$, we use a multiplier of $1/(1 + \|g\|^2)$ rather than $1/\|g\|^2$ in the variance of the Hop proposal of (5). We consider a target density which is, for each component $i = 1, \dots, d$, proportional to the product of a centred logistic density with scale σ_i and a $\mathcal{N}(0, a^2\sigma_i^2)$ density. The Gaussian ensures that the Hessian of the log target does not approach zero in the tails of the distribution; the larger a the smaller the contribution from the Gaussian. We denote this density by:

$$\pi_{LG}(x; a, \underline{\sigma}) \propto \prod_{i=1}^d \left[\exp\left(-\frac{x_i}{2\sigma_i}\right) + \exp\left(\frac{x_i}{2\sigma_i}\right) \right]^{-2} \exp\left(-\frac{1}{2} \left(\frac{x_i}{a\sigma_i}\right)^2\right). \quad (12)$$

We consider $a \in \{1, 2, 5\}$, $d \in \{10, 25, 50, 100, 250\}$, λ values between 1/8 and 64 and κ values between 1/8 and 4. We choose different types of target by changing the vector $\underline{\sigma}$: for *Iso* targets, we set $\sigma_i = 1$, whereas for *Linear* targets $\sigma_i = 10i/d$ for $i = 1, \dots, d$. In each combination of a, d, λ, κ and target type, we ran Hop for 2.5 million iterations.

Hop is designed to move between contours of $\log \pi$, and so Figure 1 shows the effective sample size of $\log \pi_{LG}(X; 0, \sigma, a)$ as a function of the choice of a, d, λ, κ and type. Firstly, whatever the target, the optimal λ increases with dimension just slightly slower than in proportion to $d^{1/2}$. By contrast the optimal κ is remarkably stable across targets and dimension, lying between 0.25 and 1. Theorem 2 does not directly describe the optimal parameter choices but it does suggest that the above patterns are necessary in order to keep the acceptance rates bounded away from 0 and 1. For each combination of dimension and target, the acceptance rates at the optimal (λ, κ) values were between 0.25 and 0.46. Moreover, all plots show that the effects of λ and κ on performance are approximately orthogonal to each other, so the reparameterisation from (λ, μ) to (λ, κ) as suggested by Theorem 2, is helpful. Finally, Hop efficiency degraded exceptionally slowly with dimension: the ratio of the optimal ESS with $d = 250$ to the optimal ESS with $d = 10$ was 0.93 for ISOLG1, 0.72 for ISOLG2, and 0.57 for ISOLG5. For the *Linear* choice of scalings the relative efficiencies were similar, respectively 0.94, 0.69 and 0.55.

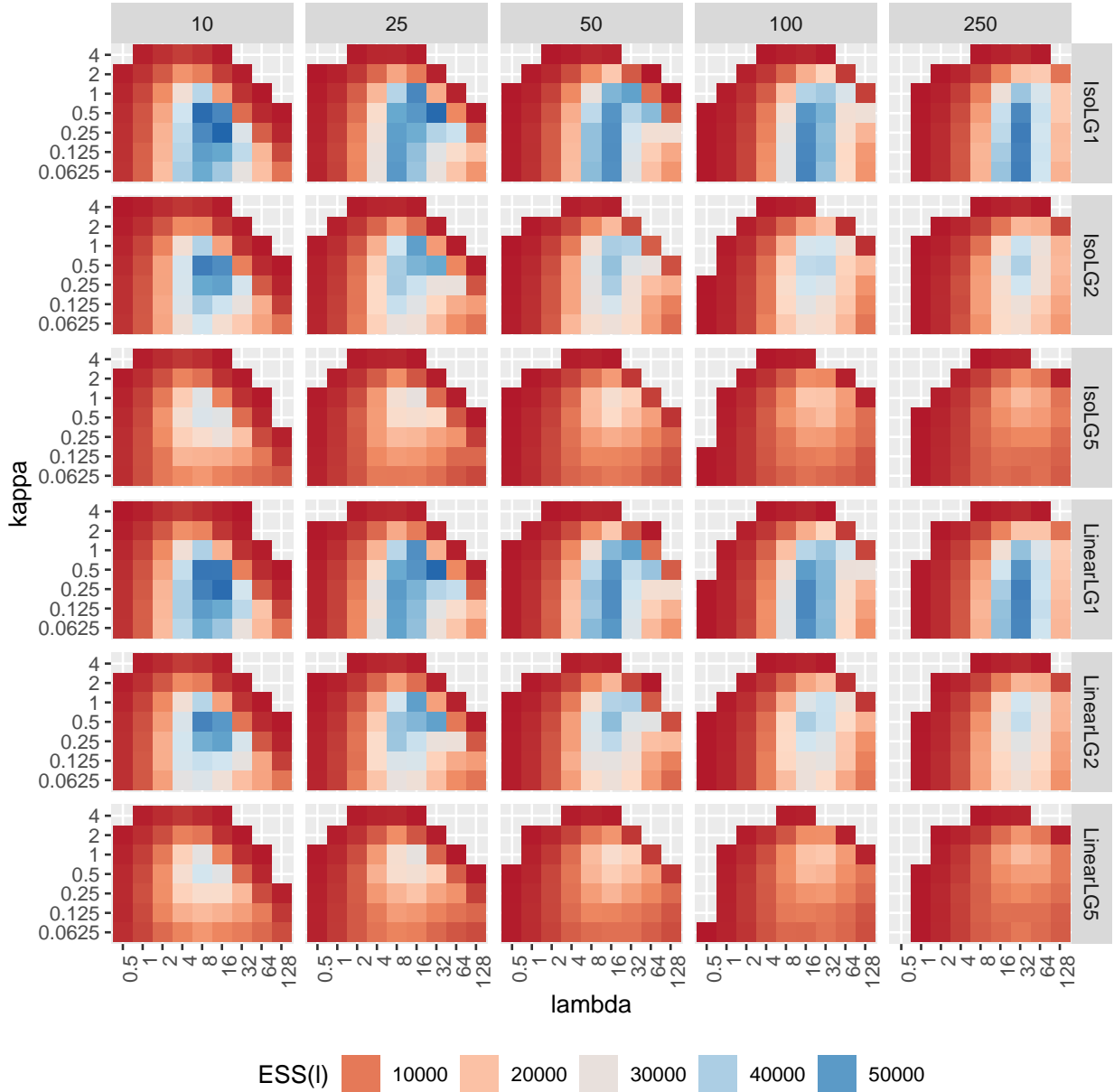


Figure 1: Effective sample size of $\ell(X)$ under *Hop* on a range of targets (rows) and dimensions (columns). Within each cell, λ and κ are varied on an logarithmic scale (base 2). Notice that LG1 targets are close to Gaussian allowing small values for κ to give close to optimal ESS values, whereas other models have an optimal $\kappa \in [0.5, 1]$.

2.3 Parallels with HMC

As with *Hug*, Hamiltonian Monte Carlo (HMC) also simulates the movement of a particle across a surface for a given time, T , using an approximation of a ‘true’ dynamic. We now discuss the similarities and differences between *Hug* and HMC. As with *Hug*, given a current position, x , standard HMC simulates a velocity from some fixed, (typically) Gaussian distribution, $V_0 \sim \mathcal{N}(0, \Sigma)$. Then, instead of approximating the dynamics in (1) via a series of B reflections, each accounting for an integration time of $\delta = T/B$, HMC approximates the Hamiltonian dynamics of a particle with an initial velocity of v_0 moving in a potential $-\ell$ via L repeats

of the Leapfrog integrator (e.g. Neal, 2011), each of which accounts for a time $\delta = T/L$:

$$v' = v_b + \frac{\delta}{2}\nabla\ell(x), \quad x_{b+1} = x_b + \delta M^{-1}v', \quad v_{b+1} = v' + \frac{\delta}{2}\nabla\ell(x_{b+1}),$$

where M is the positive-definite mass matrix. As with *Hug*, each leapfrog step is skew reversible with a Jacobian of 1, and so the kernel targets $\tilde{\pi}(x, v) = \pi(x)q(v | x)$ for exactly the same reasons as *Hug* does. Also, as with *Hug* (Theorem 1), the error in $\log \tilde{\pi}$ after integrating for a fixed time T using steps of size δ is $\mathcal{O}(\delta^2)$ (e.g. Leimkuhler et al., 2004).

An appropriate choice of M and Σ also allows for preconditioning of HMC; however, any scheme that seeks to use local Hessian information to set the mass matrix in the leapfrog step whilst maintaining skew-reversibility must be *implicit* and, hence, much more time consuming: e.g. the middle step could become: $x_{b+1} = x_b + \delta M^{-1}(\{x_b + x_{b+1}\}/2)v'$ (see also Girolami and Calderhead, 2011, for an implicit scheme which uses 3rd derivatives of ℓ). This remains true if the alternative, position-Verlet leapfrog method is used. The benefit of using local Hessian information is demonstrated in Section 3 (see also Girolami and Calderhead, 2011).

The leapfrog step is symplectic and, as a consequence, if δ is fixed and δv_0 is not too large given the curvature of $\log \pi$, then as $T = L\delta$ increases the quantity $|\ell(x_L) - \ell(x_0)|$ remains bounded (e.g. Leimkuhler et al., 2004). *Hug* is not symplectic; nonetheless, we have found empirically that, as with the leapfrog scheme, if δv_0 is not too large compared with the Hessian of $\log \pi$, as $T = B\delta$ increases, $|\ell(x_B) - \ell(x_0)|$ remains bounded; Figure 4 in Appendix B.2 demonstrates this empirically for several different targets.

Finally, the first and last steps in the leapfrog scheme depend on $g = \nabla\ell$. When $\|g\|$ is large, as, for example, in the tails of a target $\pi(x) \propto \exp(-\|x\|^4)$ then the leapfrog scheme becomes unstable and the HMC algorithm is at best unreliable. By contrast, *Hug* only depends on g via $\hat{g} = g/\|g\|$ and can remain stable even for very light-tailed targets.

2.4 Parameter tuning

Hug and *Hop* have different purposes, respectively to move in \mathcal{X} and to change $\log \pi$, and have separate parameters, respectively (T, B) and (λ, κ) . We recommend tuning the pairs of parameters separately, each with the relevant goal in mind.

For the standard *Hug*, as with HMC, T should be large enough that a reasonable distance is covered, but not so large that the proposal dynamic is likely to perform a loop, making $\|x_B - x_0\| \ll \|Tv_0\|$. Given T , δ should be chosen so that the acceptance rate is bounded away from 0 and 1. Empirical studies across a range of toy targets, dimensions and intergration times (see Appendix B.1) suggest setting δ so as to target an acceptance rate of between 60%–85%.

For *HugHess*, tuning is more complex as the term $q(v_B | x_B)/q(v_0 | x_0)$ can dominate in the calculation of the acceptance probability when there are large changes in the Hessian between x_0 and x_B . Hence, T , also might need to be reduced to ensure that the acceptance probability is bounded away from 0.

Tuning advice for *Hop* derives from Theorem 2 and the simulation study that follows it. Setting $\kappa \in (0.25, 1.0)$ leads to an acceptance probability that is bounded away from 0 and 1, and yields good performance in a range of targets. Given κ we suggest increasing λ , so as to increase the movement up or down the gradient, until this starts having a clear detrimental impact on the acceptance rate.

3 Simulation study

In this section the *Hug* and *Hop* MCMC sampler is compared to various other MCMC algorithms on a range of target distributions in $d = 25$ dimensions. We consider six classes of Model: (i) A multivariate Gaussian distribution with diagonal co-variance matrix; (ii) a product of a logistic density and a weak, regularising Gaussian density $\pi_{\text{LG}}(x; 0, 5, \underline{\sigma})$, as defined in (13); (iii) a product of a quartic and a weakly regularising Gaussian:

$$\pi_{\text{QG}}(x; a, \underline{\sigma}) \propto \prod_{i=1}^d \exp\left[-\frac{1}{2}\left(\frac{x_i}{\sigma_i}\right)^4\right] \exp\left[-\frac{1}{2}\left(\frac{x_i}{a\sigma_i}\right)^2\right] \quad (13)$$

with $a = 3$. Models (iv) - (vi) are more exotic, each consists of a $d = 25$ dimensional target with dimensions 1 and 2 independent of dimensions $3, \dots, d$, which themselves are independent, centred Gaussians. The first two dimensions are: (iv) the Banana target of (Sejdinovic et al., 2014) with banancity $b = \sqrt{2}/2$, (v) a bimodal mixture of bivariate Gaussians with separation $\lambda = 3$ or (vi) the Plus-Prism: a mixture of two bi-variate Gaussians forming a “+”-shaped target. The precise forms for the log-target, gradient and Hessian for these models can be found in Appendix D. For each target, we consider two types of scaling across the components: (U) Unit scales, where the scale parameter of each component is 1, and (L) Linear, where the scale parameter for component i is $d - i$. This yields 11 targets, since the PlusPrism with unit scales is identical to the standard Gaussian.

The following MCMC algorithms were compared: the random walk Metropolis (RWM); the RWM with Hessian-based proposal variance (e.g. Sejdinovic et al., 2014); the Metropolis-adjusted Langevin algorithm (MALA) (Besag, 1994; Roberts and Rosenthal, 1998); simplified manifold MALA (SMMALA, Girolami and Calderhead, 2011); HMC (e.g. Neal, 2011); Hug and Hop; Hug and Hop, both using Hessian information.

For each combination of target distribution and MCMC algorithm, the algorithm was tuned over a grid of parameter values to provide the best compromise between the per-second effective samples sizes (ESSs) of X and $\ell = \log \pi(X)$. For each combination the two separate measures, minimum ESS over X components and ESS for ℓ were found from a run of 2.5 million iterations with the optimal parameter choice. To compare the samplers, we consider values within each model relative to the best for that model, both per iteration and per wall-clock second.

The results, presented in Figure 2, show that, overall, in terms of ESS per second Hug and Hop (for the Unit targets) and Hug and Hop using Hessian information (for the Linear targets) are the most efficient in terms of the minimum ESS of any component, with HMC (and sometimes SMMALA) in the next tier. In contrast for the ESS of ℓ , except for a bimodal target and the Gaussian targets, HMC (and sometimes SMMALA) performs better than Hug and Hop.

4 Statistical models

In this section the utility of *Hug and Hop* is demonstrated on some some real-world models, using simulated data: a 10-dimensional cauchit regression model; an item-response, or Rash, model with 10 tests and 100 subjects; and a 256-dimensional probit regression model for binary spatial data. In each case, performance is compared against Hamiltonian Monte Carlo (HMC). Algorithm tuning and measures of efficiency are as in Section 3.

4.1 Cauchit regression

Inference for the parameters in a Generalised Linear Model (GLM) is a well-studied problem of Bayesian inference. For data consisting of binary responses, the logistic or probit link functions are popular choices, but these link functions are not robust to outliers where the linear predictor is large in absolute value (indicating the outcome is almost certain) but the linear predictor is, in fact, wrong (Koenker and Yoon, 2009). Such a situation may arise from errors in the data-recording process, for example. The “cauchit” link function is more tolerant of such outliers. The model supposes that the i th binary response, Y_i is related to the vector of M predictors for the response, x_i , through some unknown parameters, β , as follows:

$$\begin{aligned} Y_i &\stackrel{\text{iid}}{\sim} \text{Bernoulli}(p_i), \text{ for } i = 1, \dots, N \\ \mathbf{g}(p_i) &\stackrel{\text{iid}}{\sim} \beta^\top x_i, \text{ where } \mathbf{g}(u) = \tan(\pi(u - 1/2)), \\ \beta_j &\stackrel{\text{iid}}{\sim} \mathbf{N}(0, 1/\tau), \text{ for } i = 1, \dots, M. \end{aligned} \tag{14}$$

We compare Hug and Hop against HMC on data simulated from the above model with $N = 500$ data points, Y_i $i = 1, \dots, 500$, and $M = 10$ predictors $(x_{i,1}, \dots, x_{i,10})$, each of which is independently drawn from a $\mathbf{N}(0, 1)$ distribution. The optimal tunings were $L = 6$, $\epsilon = 0.6$ for HMC, $B = 5$, $T = 0.6$ for Hug and $\lambda = 6$, $\kappa = 0.6$ for Hop. The resulting efficiencies for 50,000 iterations (after a burn-in period of 50,000) are given in Table 1. This shows that by paying a small price in the efficiency of ℓ per second, the performance on X space can be more than tripled by using Hug and Hop instead of HMC.

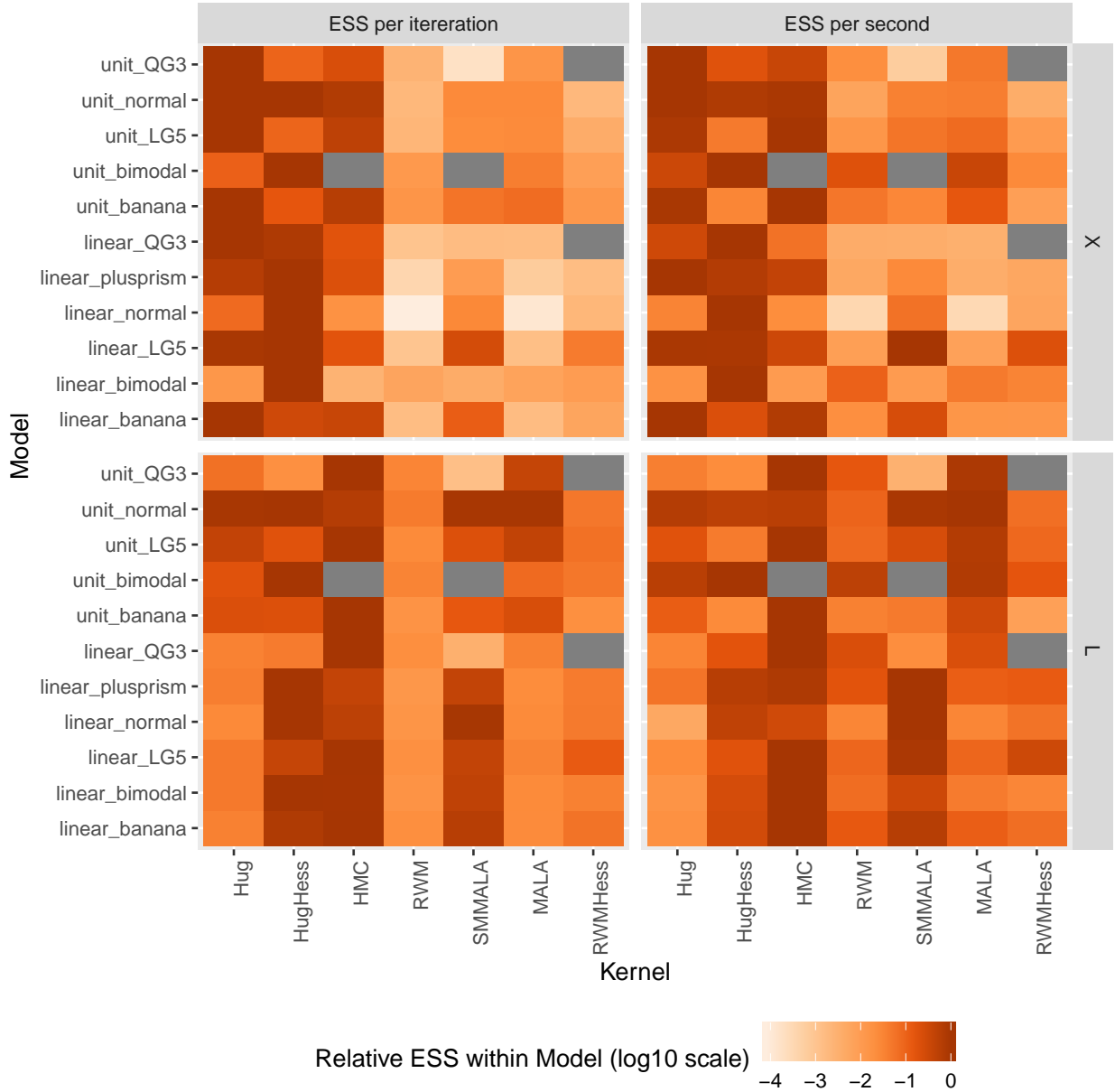


Figure 2: Comparison of effective size in $\log \pi$ (bottom) and the minimum effective size over the components of x (top) measured per MCMC iteration (left) and per wall-clock second (right). Each sampler/target pair was run for 2,500,000 iterations on a 25 dimensional target. Values are relative within each model (row of each facet) on a log10 scale. Grey indicates the kernel failed to explore the target.

4.2 Rasch model

Consider a set of M true or false questions answered by N people. Let $Y_{ij} = 1$ if person j answered question i correctly, and $Y_{ij} = 0$ otherwise. The Rasch model (Rasch, 1980) posits that the i -th question has some latent difficulty β_i and the j -th person has a latent ability η_j such that the probability person j is correct when answering question i is given by $P_{ij} = \Phi(\eta_j - \beta_i)$, where Φ is the distribution function of a standard Gaussian. Each answer Y_{ij} is thus considered as a Bernoulli outcome with probability P_{ij} . To make the model identifiable, one of the parameters must be fixed; in this case $\beta_1 = 0$ is chosen, such that a person with average ability ($\eta_j = 0$) has a 50% chance of answering question 1 correctly. Although the model is

Kernel	HMC	Hug and Hop
time (seconds)	36.6	32.1
ESS(X) per sec.	372	1166
ESS(ℓ) per sec.	459	233
ESS(X) per 1000 iter.	272	749
ESS(ℓ) per 1000 iter.	336	150

Table 1: Comparison of performance for Cauchit Regression with $M = 10$ predictors for $N = 500$ data points and prior precision τ . Both samplers ran for 50,000 iterations after discarding 50,000 as burn-in.

relatively simple, the parameters are correlated, which can degrade the performance of Gibbs-like samplers. The model has $\beta_1 = 0$ and

$$\begin{aligned}
Y_{ij} &\sim \text{Bernoulli}(\Phi(\eta_j - \beta_i)), \\
\beta_i &\stackrel{\text{iid}}{\sim} \mathbf{N}(0, \tau^{-1}) \text{ for } i = 2, \dots, M, \\
\eta_j &\stackrel{\text{iid}}{\sim} \mathbf{N}(0, \tau^{-1}) \text{ for } j = 1, \dots, N,
\end{aligned} \tag{15}$$

We simulated data from the model with $M = 10$ tests and $N = 100$ people. We set $\beta_1 = 0$, and for $i \in 2, \dots, 10$, $j \in 1, \dots, 100$, β_i and η_j were simulated independently from a $\mathbf{N}(0, 1)$ distribution. For the subsequent analysis, the priors for β_i and η_j were independent $\mathbf{N}(0, 1)$ except that, as explained above, β_1 was fixed at 0. We applied four algorithms (optimal tunings in brackets): HMC($L = 5, T = 0.5$); preconditioned HMC($L = 6, T = 0.7$) using a diagonal mass matrix M ; Hug($B = 5, T = 0.6$) and Hop($\lambda = 12, \kappa = 0.9$); Hug($B = 8, T = 1.8$) and Hop($\lambda = 20, \kappa = 0.1$), both preconditioned with a diagonal variance matrix, $\Sigma = M^{-1}$.

For the preconditioned algorithms, the elements for M relating to the β parameters were reduced by factor of $N/M = 10$ leaving the values relating to η equal to one. Each sampler was run for 50,000 iterations and 25,000 iterations discarded as burn-in before computing effective sizes. The results are given in Table 2.

Kernel	HMC	HMC-PC	Hug Hop	Hug Hop-PC
time (seconds)	22.05	25.06	23.58	27.77
α HMC or Hug	0.87	0.91	0.90	0.94
α Hop	NA	NA	0.25	0.40
ESS(X) per sec.	300	243	372	629
ESS(ℓ) per sec.	548	654	27	168
ESS(X) per 1000 iter.	265	243	351	699
ESS(ℓ) per 1000 iter.	483	655	25	187

Table 2: Effective sample sizes per 1000 iterations and per wall-clock second for the Rasch model with $M = 10, N = 100, \tau = 1$. For parameters β and η , the minima over both is reported as ESS(X). All calculations are based on 25,000 iterations after burn-in. PC denotes the use of a preconditioning matrix.

4.3 Probit spatial regression

Finally, we consider Bayesian inference for a binary spatial regression problem. Specifically, we consider a two dimensional grid of size $m \times n$. For each element (k, l) of the grid, a binary data point y_{kl} is reported. Such data sets occur when the presence or absence of a phenomena is reported; for example, diseases in epidemiology (e.g. Paciorek, 2007). We use a generalised linear geostatistical model (e.g. Diggle and Ribeiro, 2007) with a probit link function. The stationary Gaussian process that underpins the model has a variance

of $\exp(\rho)$ and uses an exponential correlation function with a range parameter of $\exp(\psi)$:

$$\begin{aligned}
\rho, \psi &\stackrel{\text{iid}}{\sim} \mathbf{N}(0, \tau^{-1}) \\
Y_g &\stackrel{\text{iid}}{\sim} \text{Bern}(\Phi(X_g)), \\
X &\sim \text{MVN}(0, \Sigma), \\
\Sigma_{gg'} &= \exp(\rho - \exp(-\psi)D_{gg'}), \\
D_{gg'} &= \sqrt{(k - k')^2 + (l - l')^2}.
\end{aligned}
\tag{16}$$

Here, X and Y are both vectors of length mn , D and Σ are $(mn) \times (mn)$ matrices, and $g = (k, l)$ and $g' = (k', l')$ are two grid cells. $\boldsymbol{\theta} = (\rho, \psi)$ is treated as an unknown parameter and, conditional on $\boldsymbol{\theta}$, the GP values X , are reparameterised to $Z = \Sigma^{-1/2}X \sim \text{MVN}(0, I)$ as in [Diggle and Ribeiro \(2007\)](#). Inference was performed via a Metropolis-within-Gibbs scheme with the Hug($B = 14, T = 1.8$) and Hop($\lambda = 9, \kappa = 0.6$) kernel applied to Z and a tuned random walk Metropolis kernel applied to $\boldsymbol{\theta}$. For comparison, we also used HMC($L = 9, T = 1.1$) in place of Hug and Hop, keeping the random walk step the same.

Using parameter values $\rho = \log(2)$ and $\psi = \log(0.2)$, we generated a 16×16 grid of data from the model in (16). We set the hyperparameters in the priors for ρ and ψ to $\tau = 1$. Each sampler ran for 250,000 iterations. The efficiencies for Z (minimum over components), $\boldsymbol{\theta}$ (minimum over ρ and ψ) and ℓ are shown in Table 3. Hug and Hop performs comparably with HMC on Z and $\boldsymbol{\theta}$, however, on ℓ HMC performs a factor of three better. Firstly, the main posterior mass of $\log \pi(X)$ has a range of approximately 130, roughly twice that which one might expect in a 258 dimensional problem if the parameter distribution were approximately Gaussian; this increases the difficulty of exploration. The increase in range is due to the two $\boldsymbol{\theta}$ components and manifests in a moderate positive correlation between ℓ and $\rho - \psi$. Furthermore, different values for $\boldsymbol{\theta}$ favour different regions for Z , and mixing for $\boldsymbol{\theta}$ under both kernels is slow compared to mixing for Z ; this combination of behaviours masks the better mixing of $Z|\boldsymbol{\theta}$ under Hug compared with HMC. For example, with $\boldsymbol{\theta}$ fixed at its posterior mode, the minimum ESS/sec for Z using Hug and Hop is over three times larger than that obtained using HMC.

Kernel	HMC	Hug and Hop
time (seconds)	850	787
α Hug or HMC	0.89	0.89
α Hop	NA	0.35
α RWM	0.395	0.398
ESS(Z) per sec.	31.7	34.2
ESS($\boldsymbol{\theta}$) per sec.	2.53	2.62
ESS(ℓ) per sec.	4.73	1.82
ESS(Z) per 1000 iter.	108	108
ESS($\boldsymbol{\theta}$) per 1000 iter.	8.59	8.27
ESS(ℓ) per 1000 iter.	16.1	5.73

Table 3: Effective sample sizes (ESS) per wall-clock second and per 1,000 iterations for the probit spacial response model. For parameters Z and $\boldsymbol{\theta}$, the minima are reported. All computations used 250,000 iterations. All results reported to three significant figures.

5 Acknowledgements

Work by both ML and CS was supported by EPSRC grant EP/P033075/1.

A Proofs of Theoretical results for Hug

A.1 Proof of Theorem 1

In this section we prove Theorem 1.

Proof. Firstly, write the difference in ℓ at x_B and x_0 as a telescoping sum and apply Equation (3):

$$\begin{aligned}
\ell(x_B) - \ell(x_0) &= \sum_{b=1}^B \ell(x_b) - \ell(x_{b-1}) && \text{[telescope]} \\
&= \frac{\delta^2}{8} \sum_{b=1}^B [v_b^\top H(x_b^-) v_b - v_{b-1}^\top H(x_{b-1}^+) v_{b-1}] && \text{[Equation (3)]} \\
&= \frac{\delta^2}{8} \left(v_B^\top H(x_B^-) v_B - v_0^\top H(x_0^+) v_0 + \sum_{b=1}^{B-1} [v_b^\top (H(x_b^-) - H(x_b^+)) v_b] \right) && (17)
\end{aligned}$$

Recall that x_b^- and x_b^+ lie on the line segment, namely the segment joining the bounce points x'_{b-1} and x'_b . Furthermore, note that $x'_b = x_b + \delta/2v_b = x'_{b-1} + \delta v_b$, therefore:

$$\|x_b^+ - x_b^-\| \leq \|x'_b - x'_{b-1}\| = \delta \|v_b\|.$$

This allows us to bound each term in the summation of (17):

$$\begin{aligned}
|v_b^\top (H(x_b^-) - H(x_b^+)) v_b| &\leq \|v_b\| \| (H(x_b^-) - H(x_b^+)) v_b \| && \text{[Cauchy-Shwartz]} \\
&\leq \|v_b\|^2 \|H(x_b^-) - H(x_b^+)\|_I && \text{[Definition of induced norm]} \\
&\leq \gamma \|v_b\|^2 \|x_b^+ - x_b^-\| && \text{[Condition 1]} \\
&\leq \gamma \delta \|v_b\|^3. && (18)
\end{aligned}$$

By Condition 2, we can also bound the first difference in (17):

$$v_B^\top H(x_B^-) v_B - v_0^\top H(x_0^+) v_0 \leq \beta (\|v_B\|^2 + \|v_0\|^2) = 2\beta \|v_0\|^2, \quad (19)$$

where we use the fact $\|v_b\| = \|v_{b-1}\|$ since reflections preserves the norm. Combining (18) and (19) in (17) with the triangle inequality results in:

$$\begin{aligned}
|\ell(x_B) - \ell(x_0)| &\leq \frac{\delta^2}{8} \left[|v_B^\top H(x_B^-) v_B - v_0^\top H(x_0^+) v_0| + \left| \sum_{b=1}^{B-1} v_b^\top (H(x_b^-) - H(x_b^+)) v_b \right| \right] \\
&\leq \frac{\delta^2}{8} \left(2\beta \|v_0\|^2 + (B-1)\gamma \delta \|v_0\|^3 \right) \\
&\leq \frac{\delta^2 \|v_0\|^2}{8} (2\beta + \gamma \|T v_0\|),
\end{aligned}$$

where the last line follows from $T = B\delta$. □

A.2 Proof of Proposition 1

Proof. Without loss of generality, set $b = 0$ and write A for $A(x'_0)$. Applying (3) but in the transformed space where the Hessian is $\tilde{H}(x) = AH(\tilde{x})A^\top$, gives

$$\begin{aligned}
|\ell(x_1) - \ell(x_0)| &= |\ell(\tilde{x}_1) - \ell(\tilde{x}_0)| \\
&= \frac{\delta^2}{8} |\tilde{v}_1^\top AH(x'_1)A^\top \tilde{v}_1 - \tilde{v}_0^\top AH(x'_0)A^\top \tilde{v}_0| \\
&\leq \frac{\delta^2}{8} |\tilde{v}_1^\top AH(x')A^\top \tilde{v}_1 - \tilde{v}_0^\top AH(x')A^\top \tilde{v}_0| \\
&\quad + \frac{\delta^2}{8} |\tilde{v}_1^\top A[H(x'_1) - H(x')]A^\top \tilde{v}_1 - \tilde{v}_0^\top A[H(x'_0) - H(x')]A^\top \tilde{v}_0| \\
&= \frac{\delta^2}{8} |v_1^\top [H(x'_1) - H(x')]v_1 - v_0^\top [H(x'_0) - H(x')]v_0| \\
&\leq \frac{\gamma\delta^3}{8} \left\{ \|v_1\|^3 + \|v_0\|^3 \right\}.
\end{aligned}$$

Here, the third line follows from the triangle inequality, the penultimate line from the fact that $AH(x')A = I_d$ and $\|\tilde{v}_1\| = \|\tilde{v}_0\|$, and the final line since $v^\top [H(b) - H(a)]v \leq \gamma \|b - a\| \|v\|^2$. \square

B Empirical exploration of the efficiency of Hug

B.1 Optimal acceptance rate

We explore the relationship between the efficiency of Hug and the acceptance rate by taking a grid of values for $T = 1, \dots, 10$ and $B = 1, \dots, 10$ on some example models in dimensions 25, 50, 75 and 100. For each value of the tuple (Model, dimension, B , T), the following procedure was performed for $i = 10,000$: (i) draw a value for x_i directly from the target; (ii) apply Hug with parameters B , T to obtain x'_i ; (iii) record $N_i = \|x'_i - x_i\|$; (iv) record $A_i = \alpha(x'_i, x_i)$.

Figure 3 shows the efficiency of Hug by plotting $\hat{\mathbb{E}}[AN^2]/dB$ against acceptance rate; the y-axis approximates the efficiency per unit time since the computational effort for an iteration is essentially proportional to B ; scaling by d is to compensate for the fact that when x has d components, $\|x\|^2 \propto d$.

B.2 Stability of hug

Figure shows a plot of $\ell(x_b) - \ell(x_0)$ against iteration number b of the inner loop in Algorithm 1 for a range of 25-dimensional models (definitions for which can be found in the main article, Section 3). *Iso* models have all scales equal to 1 while *Rand* models have scales simulated from $U(0.5, 5)$. The limits on the y -axis are chosen as double the maximum and minimum of $\ell(x_b) - \ell(x_0)$.

C Proof of Theorem 2

In proving Theorem 2 we drop the superscript (d) , whenever this is clear from the context. Since for any $d \times d$ matrix A , $y^\top Ay - x^\top Ax = (y+x)^\top A(y-x)$, substituting both the form for $\log \pi$ and that $g(x) = -\Gamma x$ into (8) gives the following.

Proposition 2. *For the d -dimensional target of Theorem 2, the acceptance ratio $r(x, y)$ satisfies*

$$2 \log r(x, y) = -C_1(x, y) + C_2(x, y) - C_3(x, y) + C_4(x, y),$$

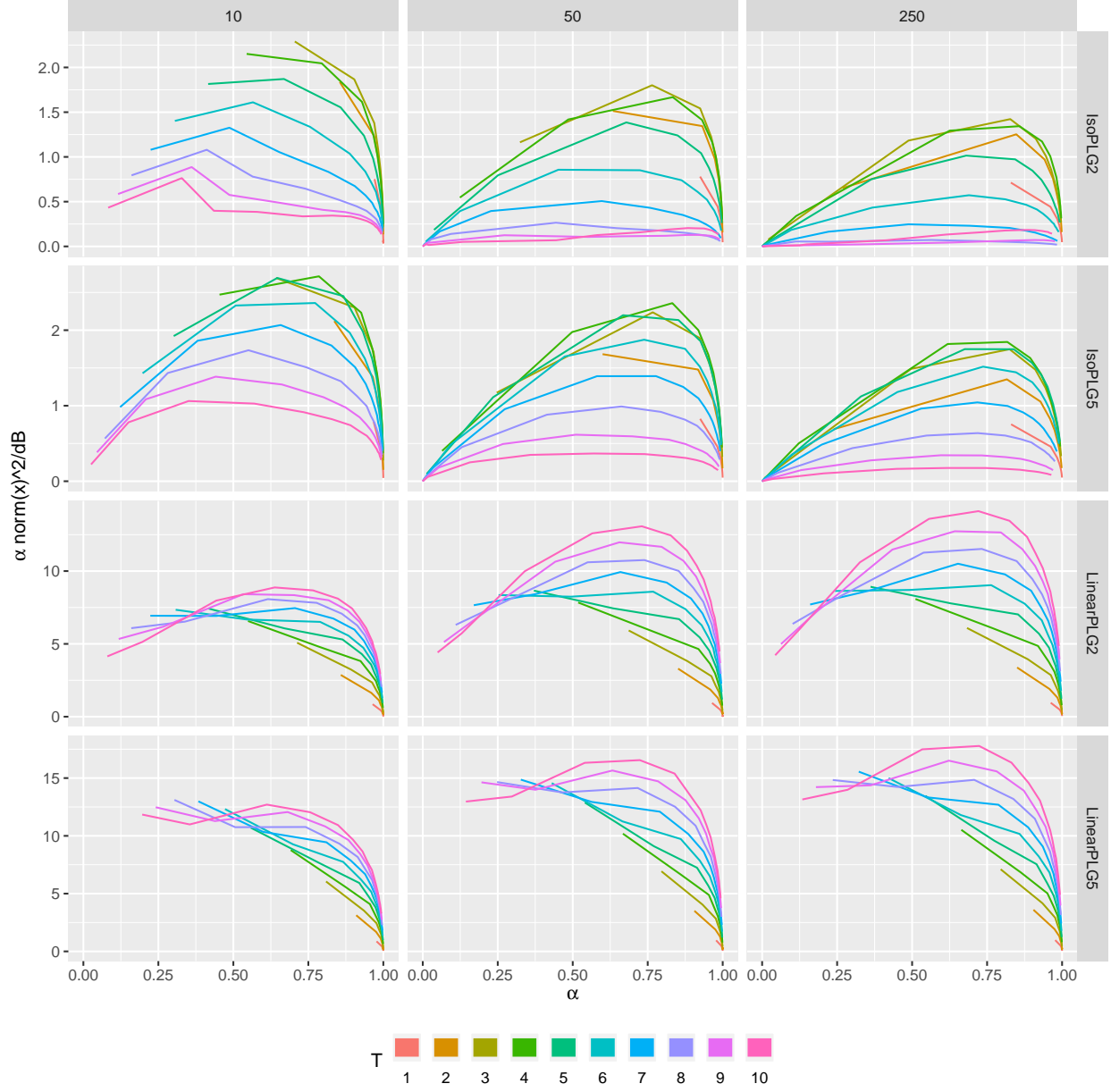


Figure 3: Efficiency plots for Hug: α vs $\alpha \|x' - x\|^2 / dB$ for a range of B s (each line) on some example models (rows) in increasing dimensions (columns) for Isotropic LG targets ($\sigma = 1$ in Equation (13)).

where

$$C_1(x, y) = (y + x)^T \Gamma(y - x) \quad (20)$$

$$C_2(x, y) = d \log \left[1 + \frac{(y + x)^T \Gamma^2(y - x)}{x^T \Gamma^2 x} \right] \quad (21)$$

$$C_3(x, y) = \frac{1}{\mu^2} \|y - x\|^2 (y + x)^T \Gamma^2(y - x) \quad (22)$$

$$C_4(x, y) = \left(\frac{1}{\mu^2} - \frac{1}{\lambda^2} \right) (y + x)^T \Gamma(y - x) (y - x)^T \Gamma(y - x). \quad (23)$$

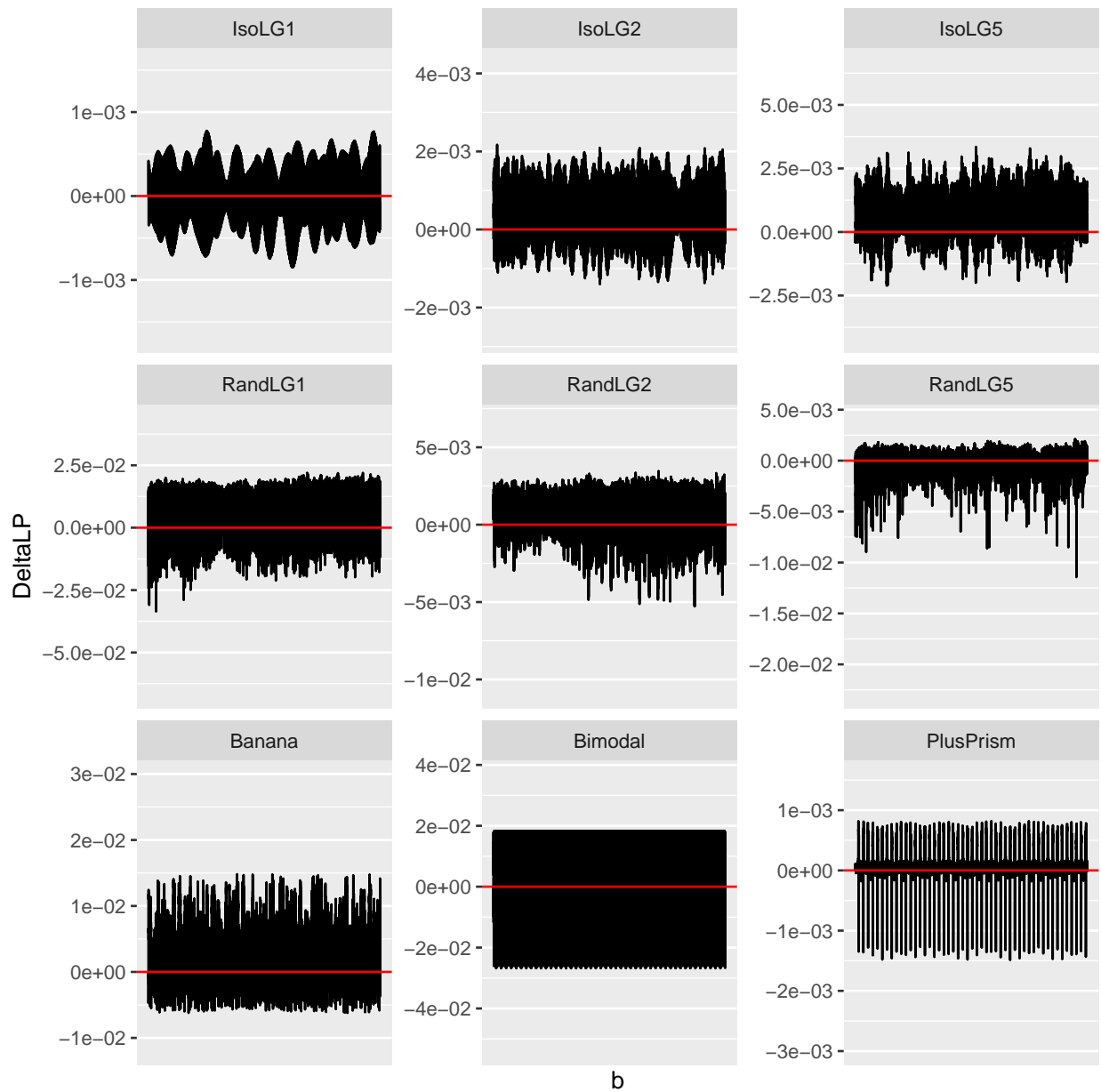


Figure 4: Stability of ℓ for various models under the *Hug* algorithm with $\delta = 0.1$. Each plot shows $\Delta_b = \ell(x_b) - \ell(x_0)$ vs. $b = 0, \dots, 10,000$ for a given 25-dimensional target. A red line through $\Delta_b = 0$ is given for reference.

We now establish the limiting behaviour of the components of the quantities in Proposition 2.

Lemma 1. *The following limits hold:*

$$\frac{\|g_X\|^2}{d} = \frac{X^\top \Gamma^2 X}{d} \xrightarrow{p} \mathbb{E}[\gamma] \quad \text{with a discrepancy of } \mathcal{O}(1/\sqrt{d}), \quad (24)$$

$$\|Y - X\|^2 \xrightarrow{p} \frac{\mu^2}{\mathbb{E}[\gamma]} \quad \text{with a discrepancy of } \mathcal{O}(\lambda/\sqrt{d}), \quad (25)$$

$$(Y - X)^\top \Gamma (Y - X) \xrightarrow{p} \mu^2 \quad \text{with a discrepancy of } \mathcal{O}(\lambda/\sqrt{d}), \quad (26)$$

$$(Y + X)^\top \Gamma (Y - X) \xrightarrow{d} 2\lambda \mathbf{N}(0, 1) + \mu^2 \quad \text{with a discrepancy of } \mathcal{O}(\lambda/\sqrt{d}), \quad (27)$$

$$(Y + X)^\top \Gamma^2 (Y - X) \quad \text{is } \mathcal{O}(\lambda). \quad (28)$$

Proof. From the form for the target, we have $X = \Gamma^{-1/2}W$, where $W \sim \text{MVN}_d(0, I_d)$ is independent of Γ .

For (24),

$$\mathbb{E}\left[\frac{1}{d}X^\top \Gamma^2 X\right] = \frac{1}{d}\mathbb{E}\left[\sum_{i=1}^d \gamma_i W_i^2\right] = \mathbb{E}[\gamma_1 W_1^2] = \mathbb{E}[\gamma].$$

$$\text{Var}\left(\frac{1}{d}X^\top \Gamma^2 X\right) = \frac{1}{d^2}\text{Var}\left(\sum_{i=1}^d \gamma_i W_i^2\right) = \frac{1}{d}\text{Var}(\gamma_1 W_1^2) \leq \frac{1}{d}\mathbb{E}[\gamma_1^2 W_1^2] = \frac{3}{d}\mathbb{E}[\gamma^2],$$

and $\mathbb{E}[\gamma^2] < \infty$, giving the required result.

From the form for the proposal, (5), and (7) we have

$$Y - X = \frac{1}{\|g_X\|} \left[\mu Z + (\lambda - \mu) \frac{g_X}{\|g_X\|} (\widehat{g}_X^\top Z) \right].$$

where $Z \sim \text{MVN}_d(0, I_d)$ is independent of W and Γ . But $g_X = \Gamma X = \Gamma^{1/2}W$. Define $A := \widehat{g}_X^\top Z \sim \mathbf{N}(0, 1)$ since it is a single (albeit random) component of the isotropic standard Gaussian. Substituting for X and g_X , for each $a \in \{0, 1, 2\}$,

$$\begin{aligned} T_1(a) &:= (Y - X)^\top \Gamma^a (Y - X) \\ &= \mu^2 \frac{Z^\top \Gamma^a Z}{W^\top \Gamma W} + 2\mu(\lambda - \mu)A \frac{W^\top \Gamma^{a+1/2} Z}{(W^\top \Gamma W)^{3/2}} + (\lambda - \mu)^2 A^2 \frac{W^\top \Gamma^{a+1} W}{(W^\top \Gamma W)^2} \\ &\xrightarrow{p} \mu^2 \frac{\mathbb{E}[\gamma^a]}{\mathbb{E}[\gamma]}. \end{aligned}$$

Consider each of the fractions above (that is, ignoring the λ and μ parts). The third fraction has a numerator of $\mathcal{O}(d)$ yet the denominator is $\mathcal{O}(d^2)$, so the term is $\mathcal{O}((\lambda - \mu)^2/d) = \mathcal{O}(\lambda^2/d)$. When $a \in \{0, 1\}$ the second fraction an expectation of 0 and a variance of $\mathcal{O}(1/d^2)$, so the term is at most $\mathcal{O}(\mu(\lambda - \mu)/d) = \mathcal{O}(\lambda^{3/2}/d) = o(\lambda/\sqrt{d})$. When $a = 2$ the fraction has a numerator of at most $\mathcal{O}(d)$ and so the whole term is $\mathcal{O}(\lambda^{3/2}/d^{1/2}) = o(\lambda)$. The first term converges in probability to $\mu^2/\mathbb{E}[\gamma]$ if $a = 0$ and $\mu^2\mathbb{E}[\gamma^2]/\mathbb{E}[\gamma]$ if $a = 2$, each with deviations of $\mathcal{O}(\mu^2/\sqrt{d}) = \mathcal{O}(\lambda/\sqrt{d})$; when $a = 1$ the first term is exactly μ^2 . This proves (25) and (26).

For $a \in \{1, 2\}$,

$$\begin{aligned} T_2(a) &:= 2X^\top \Gamma^a (Y - X) \\ &= 2\mu \frac{W^\top \Gamma^{a-1/2} Z}{(W^\top \Gamma W)^{1/2}} + 2(\lambda - \mu)A \frac{W^\top \Gamma^a W}{W^\top \Gamma W}. \end{aligned}$$

When $a = 1$, the first term is $2\mu\widehat{g}_X^\top Z = 2\mu A$, and the second term is $2(\lambda - \mu)A$ so $T_2(1) = 2\lambda\mathbf{N}(0, 1)$; combining this with (26) proves (27). When $a = 2$, the first fraction has a squared expectation of $\mathcal{O}(1)$, so the entire first term is $\mathcal{O}(\mu) = \mathcal{O}(\sqrt{\lambda})$. The second fraction is also $\mathcal{O}(1)$ and so the second term is $\mathcal{O}(\lambda)$. Combining the results for $T_1(2)$ and $T_2(2)$ gives (28). \square

Proof of Theorem 2. Let $R := (Y + X)^\top \Gamma^2 (Y - X) / X^\top \Gamma^2 X$. By Lemma 1 lines (24) and (28) $dR^2 \xrightarrow{p} 0$ with discrepancies of $\mathcal{O}(\lambda^2/d)$. By Taylor's remainder theorem: $d \log(1+R) = dR - \frac{dR^2}{2\eta^2}$ for some $\eta \in (1-R, 1+R)$. Thus, since $R \xrightarrow{p} 0$,

$$d \log(1+R) - dR \xrightarrow{p} 0 \quad \text{with discrepancies of } \mathcal{O}(\lambda^2/d) = o(\lambda/\sqrt{d}).$$

Hence, up to a discrepancy of $\mathcal{O}(\lambda/\sqrt{d})$,

$$C_2(X, Y) - C_3(X, Y) = \left\{ \frac{1}{X^\top \Gamma^2 X} - \frac{1}{\mu^2} \|Y - X\|^2 \right\} (Y + X)^\top \Gamma^2 (Y - X).$$

By (24) and (25) the term in curly braces $\xrightarrow{p} 0$ with a discrepancy of $\mathcal{O}(1/\sqrt{d})$. Combining this with (28) we see that $C_2(X, Y) - C_3(X, Y) \xrightarrow{p} 0$ with a discrepancy of $\mathcal{O}(\lambda/\sqrt{d})$.

Furthermore,

$$C_4(X, Y) - C_1(X, Y) = \left\{ \left(\frac{1}{\mu^2} - \frac{1}{\lambda^2} \right) (Y - X)^\top \Gamma (Y - X) - 1 \right\} (Y + X)^\top \Gamma (Y - X).$$

From (26) the term in curly braces $\xrightarrow{p} -\mu^2/\lambda^2$ with a discrepancy of $\mathcal{O}(1/\sqrt{d})$, and from (27) the multiplicand $\xrightarrow{p} 2\lambda\mathbf{N}(0, 1) + \mu^2$ with a discrepancy of $\mathcal{O}(\lambda/\sqrt{d})$. Hence

$$C_4(X, Y) - C_1(X, Y) \xrightarrow{p} -\frac{\mu^4}{\lambda^2} + 2\frac{\mu^2}{\lambda}\mathbf{N}(0, 1),$$

with a discrepancy of $\mathcal{O}(\lambda/\sqrt{d})$. Equivalently

$$\log r(X, Y) \xrightarrow{p} -\frac{1}{2}\kappa^2 + \kappa\mathbf{N}(0, 1), \tag{29}$$

with a discrepancy of $\mathcal{O}(\lambda/\sqrt{d})$.

Since $h(x) := 1 \wedge \exp(x)$ is bounded and continuous, we obtain

$$\mathbb{E}[h(r(X, Y))] \rightarrow \mathbb{E}\left[1 \wedge \exp\left(-\frac{1}{2}\kappa^2 + \kappa A\right)\right],$$

where $A \sim \mathbf{N}(0, 1)$. Proposition 2.4 in Roberts et al. (1997) then gives (9).

For the final result, notice that $0 \leq h(x) \leq 1$ and $h(x)$ is Lipschitz-continuous with a Lipschitz constant of 1. Let (X, Y) have distribution ν , let $A(X, Y) \sim \mathbf{N}(0, 1)$ be the Gaussian in (29). Given $c > 0$, let $\mathcal{B} := \{(X, Y) : |\log(r(X, Y) + \kappa^2/2 - \kappa A(X, Y))| > c\lambda/\sqrt{d}\}$. Since discrepancies from the limit in (29) are $\mathcal{O}(\lambda/\sqrt{d})$ we may choose c such that $\mathbb{P}(\mathcal{B}) < c\lambda/\sqrt{d}$. The bounds on h give

$$\int_{\mathcal{B}} |h(\log r(x, y)) - h(-\kappa^2/2 + \kappa A(x, y))| \nu(\mathbf{d}x, \mathbf{d}y) < c\lambda/\sqrt{d},$$

and the Lipschitz continuity of h gives

$$\int_{\mathcal{B}^c} |h(\log r(x, y)) - h(-\kappa^2/2 + \kappa A(x, y))| \nu(\mathbf{d}x, \mathbf{d}y) < c\lambda/\sqrt{d}.$$

Thus, by the triangle inequality, $|\mathbb{E}[h(r(X, Y))] - \mathbb{E}[h(-\kappa^2/2 + \kappa A)]| < 2c\lambda/\sqrt{d}$. \square

D Example targets

D.1 Banana

The Banana(a, c, b) target has a centred Normal distribution with scale a in the first dimension. Letting, $s = c\sqrt{1-b^2}$ and $r = \frac{bc\sqrt{2}}{2a^2}$, the second dimension, conditional on the first has distribution:

$$X_2 | (X_1 = x_1) \sim \mathbf{N}(r(x_1^2 - a^2), s).$$

Note that $\text{Var}(X_2) = c^2$ and $b \in (0, 1)$. The parameter b is the *bananacity* of the target, larger values for b make the banana bendier, whilst at $b = 0$ then $r = 0$ and the model degenerates to a product of independent normal distributions. We take $b = \sqrt{2}/2$ unless otherwise stated. The log-target for this model is thus:

$$\log \pi(x) = -\frac{x_1^2}{2a^2} - \frac{(x_2 - r(x_1^2 - a^2))^2}{2s^2}.$$

D.2 Bimodal

The Bimodal(a, b, λ) target is an equal mixture of two bi-variate Normal distributions, $\text{MVN}(\mu, \Sigma)$ and $\text{MVN}(-\mu, \Sigma)$, where

$$\mu = \left(a\sqrt{1 - 1/\lambda^2}, b\sqrt{1 - 1/\lambda^2} \right) \text{ and } \Sigma = \text{diag} \left((a/\lambda)^2, (b/\lambda)^2 \right).$$

The marginal scales of a Bimodal(a, b, λ) are a and b ; and that the expectation is $\mathbf{0}$. The *separation parameter* $\lambda \geq 1$ acts to “push” the components apart while keeping the scales of the marginals equal to a and b . The default values for λ in our experiments is 3.

D.3 PlusPrism

The PlusPrism(a, b) target is given by an equal mixture of two centred bi-variate Normal distributions with covariance matrices Σ_1 and Σ_2 given by

$$\Sigma_1 = \text{diag} (2a^2 - 1, 1) \text{ and } \Sigma_2 = \text{diag} (1, b^2 - 1).$$

This target has mass spread in a “+” shape along the x and y axis with a mode at $(0,0)$. In three or more dimensions, this two-dimensional plus is projected along the other dimensions creating a prism. The marginal scales of PlusPrism(a, b) are a and b .

E Statistical model calculations

E.1 Cauchit regression

To simplify the formulae, we redefine the response to be $Y_i \in \{-1, 1\}$ rather than $Y_i \in \{0, 1\}$. The inverse link function is $g^{-1}(x) = 1/2 + \text{atan}(x)/\pi$, where, here only, π is the number 3.14... Now, $g^{-1}(-x) = 1 - g^{-1}(x)$, and writing $z_i = y_i x_i^\top \beta$,

$$\begin{aligned} \ell(\beta) &= -\frac{\tau}{2} \|\beta\|^2 + \sum_i \log(1/2 + \text{atan}(z_i)/\pi), \\ \frac{\partial \ell}{\partial \beta_j} &= -\tau \beta_j + \sum_i \frac{y_i x_{ij}}{(1 + z_i^2)(\pi/2 + \text{atan}(z_i))}. \end{aligned}$$

E.2 Rasch model

As with the cauchit regression we redefine the response to be $Y_{ij} \in \{-1, 1\}$ and let $z_{ij} = y_{ij}(\eta_j - \beta_i)$. Then:

$$\begin{aligned} \ell(\beta, \eta | y) &= \sum_{ij} \log \Phi(z_{ij}) - \frac{\tau}{2} \sum_i \beta_i^2 - \frac{\tau}{2} \sum_j \eta_j^2, \\ \frac{\partial \ell}{\partial \beta_i} &= \sum_j -y_{ij} \frac{\phi(z_{ij})}{\Phi(z_{ij})} - \tau \beta_i, \\ \frac{\partial \ell}{\partial \eta_j} &= \sum_i y_{ij} \frac{\phi(z_{ij})}{\Phi(z_{ij})} - \tau \eta_j. \end{aligned}$$

E.3 Probit Spatial Regression

Recall the model in Equation (16) and the reparameterisation into (Z, θ) . Let $[Av]_i$ denote the i th element of vector resulting from the matrix product Av and $\Sigma = A^T A$. Then $\text{Var}(X) = \text{Var}(A^T Z) = \Sigma$. With $Y_g \in \{-1, 1\}$, we obtain as the log-target:

$$\ell(\rho, \psi, z|y) = \sum_g \log \Phi(y_g [A^T z]_g) - \frac{1}{2} z^T z - \frac{1}{2} \rho^2 - \frac{1}{2} \psi^2,$$

and the gradient with respect to a component of z is

$$\frac{\partial \ell}{\partial z_j} = -z_j + \sum_g y_g A_{gj}^T \frac{\phi(y_g [A^T z]_g)}{\Phi(y_g [A^T z]_g)}.$$

References

- Besag, J. (1994). In discussion of ‘Representations of knowledge in complex systems’ by U. Grenander and M. Miller. *J. Roy. Stat. Soc. Ser. B*, 56:591–592.
- Bierkens, J. (2015). Non-reversible metropolis-hastings. *Statistics and Computing*, 26(6):1213–1228.
- Bierkens, J., Kamatani, K., and Roberts, G. O. (2018). High-dimensional scaling limits of piecewise deterministic sampling algorithms. *arXiv preprint arXiv:1807.11358*.
- Bouchard-Côté, A., Vollmer, S. J., and Doucet, A. (2018). The bouncy particle sampler: A non-reversible rejection-free markov chain monte carlo method. *Journal of the American Statistical Association*, 113(522):855–867.
- Brooks, S., Gelman, A., Jones, G., and Meng, X.-L. (2011). *Handbook of markov chain monte carlo*. CRC press.
- Diaconis, P., Holmes, S., and Neal, R. M. (2000). Analysis of a nonreversible markov chain sampler. *The Annals of Applied Probability*, 10(3):726–752.
- Diggle, P. and Ribeiro, P. (2007). *Model-based Geostatistics*. Springer Series in Statistics. Springer.
- Fearnhead, P., Bierkens, J., Pollock, M., and Roberts, G. O. (2018). Piecewise deterministic markov processes for continuous-time monte carlo. *Statistical Science*, 33(3):386–412.
- Girolami, M. and Calderhead, B. (2011). Riemann manifold langevin and hamiltonian monte carlo methods. *Journal of the Royal Statistical Society: Series B (Statistical Methodology)*, 73(2):123–214.
- Hastings, W. K. (1970). Monte carlo sampling methods using markov chains and their applications. *Biometrika*, 57(1):97–109.
- Koenker, R. and Yoon, J. (2009). Parametric links for binary choice models: A fisherian – bayesian colloquy. *Journal of Econometrics*, 152(2):120–130.
- Leimkuhler, B., Reich, S., and Press, C. U. (2004). *Simulating Hamiltonian Dynamics*. Cambridge Monographs on Applied and Computational Mathematics. Cambridge University Press.
- Ma, Y.-A., Fox, E. B., Chen, T., and Wu, L. (2018). Irreversible samplers from jump and continuous markov processes. *Statistics and Computing*.
- Mallik, A. and Jones, G. L. (2017). Directional metropolis-hastings. *arXiv preprint arXiv:1710.09759*.
- Neal, R. M. (1998). Suppressing random walks in markov chain monte carlo using ordered overrelaxation. In *Learning in Graphical Models*, pages 205–228. Springer Netherlands.

- Neal, R. M. (2011). Mcmc using hamiltonian dynamics. In Brooks, S., Gelman, A., Jones, G., and Meng, X.-L., editors, *Handbook of markov chain monte carlo*, chapter 5, pages 113–162. CRC press.
- Paciorek, C. J. (2007). Computational techniques for spatial logistic regression with large data sets. *Computational Statistics & Data Analysis*, 51(8):3631–3653.
- Peters, E. A. J. F. and de With, G. (2012). Rejection-free monte carlo sampling for general potentials. *Phys. Rev. E*, 85:026703.
- Rasch, G. (1980). *Probabilistic models for some intelligence and attainment tests*. University of Chicago Press, Chicago, expanded ed. edition.
- Roberts, G. O., Gelman, A., Gilks, W. R., et al. (1997). Weak convergence and optimal scaling of random walk metropolis algorithms. *The annals of applied probability*, 7(1):110–120.
- Roberts, G. O. and Rosenthal, J. S. (1998). Optimal scaling of discrete approximations to langevin diffusions. *Journal of the Royal Statistical Society: Series B (Statistical Methodology)*, 60(1):255–268.
- Roberts, G. O. and Rosenthal, J. S. (2001). Optimal scaling for various metropolis-hastings algorithms. *Statist. Sci.*, 16(4):351–367.
- Sejdinovic, D., Strathmann, H., Garcia, M. L., Andrieu, C., and Gretton, A. (2014). Kernel adaptive metropolis-hastings. In *International Conference on Machine Learning*, pages 1665–1673.
- Sherlock, C., Fearnhead, P., and Roberts, G. O. (2010). The random walk metropolis: Linking theory and practice through a case study. *Statist. Sci.*, 25(2):172–190.
- Sherlock, C. and Thiery, A. H. (2017). A discrete bouncy particle sampler. *arXiv preprint arXiv:1707.05200*.
- Vanetti, P., Bouchard-Côté, A., Deligiannidis, G., and Doucet, A. (2017). Piecewise deterministic markov chain monte carlo. *arXiv preprint arXiv:1707.05296*.
- Wu, C. and Robert, C. P. (2018). The coordinate sampler: A non-reversible gibbs-like mcmc sampler. *arXiv preprint arXiv:1809.03388*.